

# Physical and Magnetic Properties of Nanocrystalline Mn Substituted Li-ferrite

A.A.Sattar <sup>a,\*</sup>, W.R.Agami<sup>a</sup>, M.A.Ashmawy<sup>b</sup> and A.A.Ghani <sup>a</sup>

<sup>a</sup> Department of Physics, Faculty of Science, Ain Shams University 11566  
Abbassia, Cairo, Egypt.

<sup>b</sup>Department of Basic Science, Faculty of Engineering , Modern Academy,  
El Mokatam, Cairo, Egypt.  
Adel\_Sattar@maktoob.com

*Nanoparticles of spinel ferrite of the chemical composition  $Li_{0.5-0.5x}Mn_xFe_{2.5-0.5x}O_4$  ;  $x= 0, 0.25, 0.5, 0.75$  and  $1$  were prepared by sol-gel autocombustion technique. The effect of  $Mn_{+2}$  –ions on crystalline phase formation ,morphology, cation distribution and magnetic properties of Li-ferrite were investigated by X-ray diffraction (XRD), Transmission electron microscopy (TEM), IR spectroscopy and Vibrating sample magnetometer (VSM) .Also the effect of heat treatment on microstructure of  $Li_{0.5}Fe_{2.5}O_4(x=0)$  has been correlated to magnetic properties whereas the well crystallinity and single phase are confirmed by X-ray and TEM for annealing temperature ( $T_a=400,600,800$ ) .It's observed that the addition of  $Mn_{+2}$  – ions promotes the saturation magnetization( $M_s$ ) until ( $x=0.5$ ), then appreciable decrease occurs due to Yafet-Kittel arrangement. The decrease in Curie temperature ( $T_c$ ) was remarkable. So, the substitution of  $Mn_{+2}$  – ions plays an important role in changing the physical and magnetic properties of lithium-manganese ferrites.*

## 1. Introduction.

The polycrystalline ferrites have very important electric, magnetic and optical properties that are dependent on several factors such as method of preparation, substituted cations, microstructure, etc. Lithium ferrite as well as substituted lithium ferrite has interesting technological applications such as cathode materials in lithium ion batteries [1–3]. They are used in microwave applications such as circulators, switches, cores of high frequency inductors. Moreover they have high ( $T_c$ ), thermal stability, excellent squareness and economical price [4-5]. The conventional way of producing these materials is by the solid state reaction. This method has some inherent disadvantages such as (1) chemical inhomogeneity, (2) coarser particle size, and (3) introduction of impurities during ball milling [6]. Furthermore, precipitation of  $\alpha$ - $Fe_2O_3$  or the

formation of  $\text{Fe}_3\text{O}_4$  may occur [7]. Various synthesizing methods have been reported, including co-precipitation, hydrothermal synthesis, and sol–gel methods [8-10].

However, these methods are economically unfeasible for large-scale production. Recently more attention has been paid to the citrate–nitrate precursor auto-combustion method, which allows producing ultra-fine powders with chemically homogeneous composition, uniform size and good reactivity [11 and 12]. Several investigations on Mn-substituted lithium ferrite with formula  $(\text{Li}_{0.5}\text{Mn}_x\text{Fe}_{2.5-x}\text{O}_4)$  have been carried out [13-16]. However according to our literature survey there are no studies concerned with the magnetic and structural properties of nanocrystalline  $(\text{Li}_{0.5-0.5x}\text{Mn}_x\text{Fe}_{2.5-0.5x}\text{O}_4)$  prepared by sol-gel autocombustion method.

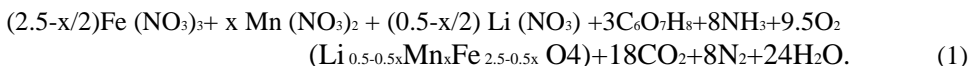
Therefore, in the present work, the influence of  $\text{Mn}^{+2}$  –ions substituted Li-ferrite  $\text{Li}_{0.5-0.5x}\text{Mn}_x\text{Fe}_{2.5-0.5x}\text{O}_4$ ;  $x= 0, 0.25, 0.5, 0.75$  and 1 on structural, cation distribution and magnetic properties of samples prepared by sol-gel autocombustion method is reported. Moreover, pure Li-ferrite treated at different annealing temperature  $T_a$  (400, 600 and 800 °C) was studied.

## 2. Experimental

### 2.1. Sample Preparation.

The spinel ferrites having composition  $\text{Li}_{0.5-0.5x}\text{Mn}_x\text{Fe}_{2.5-0.5x}\text{O}_4$ ;  $x=0, 0.25, 0.5, 0.75$  and 1 were prepared by sol-gel autocombustion method.

Analytical grade lithium nitrate, manganese nitrate and ferric nitrate were taken in stoichiometric proportion and were dissolved in deionized water with subsequent addition of citric acid. The ratio of citric acid to total metal nitrates was 1:1. Ammonia was then added until the pH of the solution reached 8.3. The detailed processes of sol-gel autocombustion method are given in the flow chart of Fig. (1). Complete synthesis detail is available elsewhere [17 -19]. The produced magnetic phase by sol-gel autocombustion process may follow the chemical reaction:



The as prepared  $\text{Li}_{0.5}\text{Fe}_{2.5}\text{O}_4$  i.e. at  $x=0$  was mixed with a few droplets of water as a binder and pressed under uniaxial pressure of 6 ton/cm<sup>2</sup>. The samples were annealed at 400°C, 600°C and 800 °C for 1 hour at atmospheric pressure.

### 2.2. Physical Characteristics.

#### 2.2.1. X-ray diffraction and morphology studies.

X-ray diffraction (XRD) patterns of all samples were taken at room temperature on Philips X`Pert Graphics and Identify using Cu – $K\alpha$  radiation ( $\lambda=1.54056 \text{ \AA}$ ). The lattice parameter (a) was calculated from the relation

$a=d_{hkl} \cdot (h^2+k^2+l^2)^{1/2}$ . The values of lattice parameters obtained for each reflected plane are plotted against the function  $F(\theta) = 1/2([\cos^2\theta/\sin\theta + \cos^2\theta/\theta])$ ;  $\theta$  is Bragg's angle, where straight lines were obtained. The accurate values of  $(a)$  were determined from extrapolation of these lines to  $F(\theta)=0$  [20]. The particle size was calculated from the line broadening analysis (XLBA), employing Debye-Scherrer formula [21]:

$$D=K\lambda/\beta\cos\theta \quad (2)$$

Where  $K$  is a constant that depends on the shape of particle;  $K=0.9$ ,  $\lambda$  is the X-ray wavelength,  $\beta$  is the full width at half maximum for each peak and  $\theta$  is the corresponding diffraction angle. The theoretical X-ray density,  $d_x$  of all samples was calculated according to the formula ( $d_x = 8M/Na^3$ ) where  $M$  is the molecular weight,  $N$  is Avogadro's number and  $a$  is the lattice parameter. The practical density,  $d$ , of each sample was measured in bidistilled water using Archimedes principle. The porosity percentage ( $P\%$ ) was calculated according to the relation:

$$P=100(1-d/d_x) \quad (3)$$

The surface area ( $S$ ) is calculated from the relation [22]:

$$S=6/Ld_x \quad (4)$$

where  $L$  is the particle size. The powder morphology was investigated by Transmission Electron Microscope (TEM, JEOL JEM-100CX) with accelerating voltage up to 100 KeV. The average particle size was estimated from TEM images.

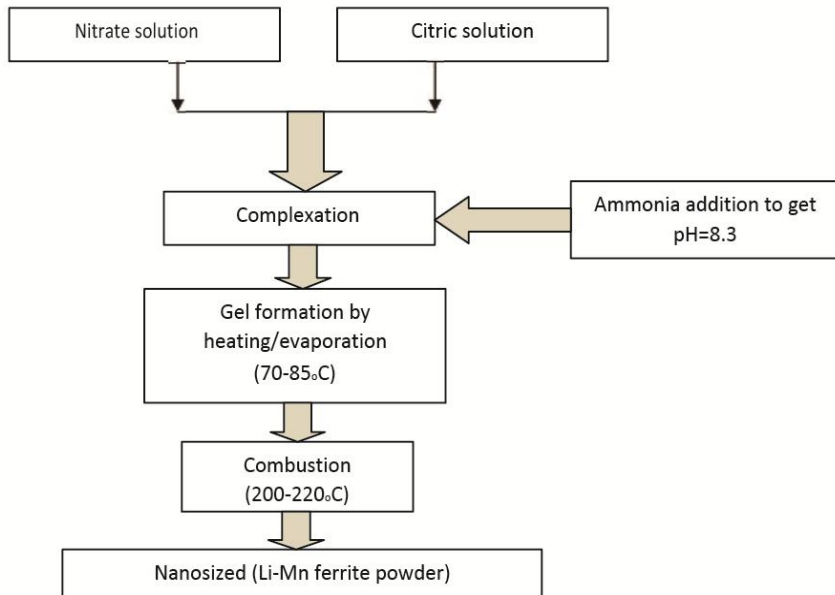


**Fig.(1):** Flow chart of sol-gel autocombustion process.

### 2.2.2. Infrared Spectroscopy Measurements.

Infrared transmission spectra of all as prepared samples of  $(Li_{0.5-0.5x}Mn_xFe_{2.5-0.5x}O_4)$  and  $(Li_{0.5}Fe_{2.5}O_4)$  annealed at different temperatures, 400,600 and 800°C, were recorded in KBr medium in the wavenumber range 200-1000  $cm^{-1}$  with a PERKIN ELMER 1430 Ratio Recording IR spectroscopy.

### 2.3. Magnetic Measurements.

The magnetization was measured on powder samples, at room temperature by Vibrating Sample Magnetometer (VSM, EG&G PARC model no.1551 USA). Toroidal samples were used as transformer cores to determine the Curie temperature  $T_c$ .

## 3. Results and Discussion

### 3.1. Physical Studies.

#### 3.1.1. X-ray Diffraction Analysis.

The XRD patterns of as prepared  $Li_{0.5-0.5x}Mn_xFe_{2.5-0.5x}O_4$  samples are shown in Fig. (2), where the XRD peaks showed a single-phase spinel ferrite structure. It is also observed that all reflections are shifted to lower values, which implies a change in lattice parameter due to Mn doping. Fig. (3), shows that the increase in the annealing temperature for pure  $Li_{0.5}Fe_{2.5}O_4$  ferrite yields more sharp peaks, i.e. an increase of the grain size as well as the crystallinity. The lattice constant  $a$  ( $A_o$ ) calculated from XRD data is found to increase with increasing of Mn concentration as in (Fig.4). The increase in lattice parameter is attributed to the difference in ionic radii, where the ionic radius of  $Mn_{+2}$ -ion is larger than the average ionic radii of  $Fe_{+3}$  and  $Li_{+1}$  (the ionic radii of  $Mn_{+2}$ ,  $Li_{+1}$  and  $Fe_{+3}$  are 0.66  $A_o$ , 0.59  $A_o$  and 0.49  $A_o$  respectively in the tetrahedral site and 0.83  $A_o$ , 0.76  $A_o$  and 0.645  $A_o$  respectively in the octahedral site) [23]. Furthermore, the lattice parameter of the annealed samples is nearly constant as shown in (Fig.5), which indicates that the annealing temperature is so small to affect the lattice parameter. Fig.(6), shows the variation of the particle size, calculated from XRD, as function of Mn concentration  $x$ . It is clear that the particle size decreased at first on addition of  $Mn_{+2}$  and remained almost constant in the Li-Mn series and then decreased again at Mn-ferrite. The same behavior of particle size was observed by introducing  $Mn_{+2}$ -ion to Ni and Co-ferrites by many authors [24 and 25]. The variation of particle size with addition of  $Mn_{+2}$ -ion could be discussed as follows:

Sol gel autocombustion reactions consist of a nucleation step followed by particle growth stages in the citrate ion network. The nucleation step occurs when the simultaneous reactions of hydrolysis and condensation occur. The addition of ammonia solution and raising the temperature help condensation process which in turn increases the nucleation rate in the citrate ion network. In the ferrite system,

the critical radius ( $r^*$ ) of the nucleated particle and the structure depends on the individual properties of the metal ions (such as solubility product  $K_{sp}$  of the metal hydroxide  $M(OH)_n$ [hydrolysis process]) and the pathway to thermodynamically stable metal ferrite [condensation process]. These two processes have a vital role in the growth process. The calculated average size of  $Li_{0.5-0.5x} Mn_x Fe_{2.5-0.5x} O_4$ ;  $x = 0, 0.25, 0.5, 0.75$  and  $1$  particles are  $61.6, 40, 42.2, 42.3$  and  $33$  nm respectively. Though all these samples are synthesized under identical conditions (reaction temperature, pH, solvent, etc.), the large variation of the average particle size by introducing the  $Mn_{+2}$ -ion shows that the concentration of the divalent metal ions has a strong influence on the particle size, such that, as  $K_{sp}$  value increases the particle size increases also[26]. In our case the ferric hydroxide formation ( $K_{SP} \sim 10^{-39}$ ) is common in all ferrite ions. So the size variation can be attributed to  $K_{SP}$  values of  $M(OH)_n$ . As Lithium hydroxide solubility product is ( $K_{SP} \sim 28$ ) and manganese hydroxide solubility product is ( $K_{SP} \sim 10^{-9}$ ), it is expected that the particle size decreases which we are found experimentally.

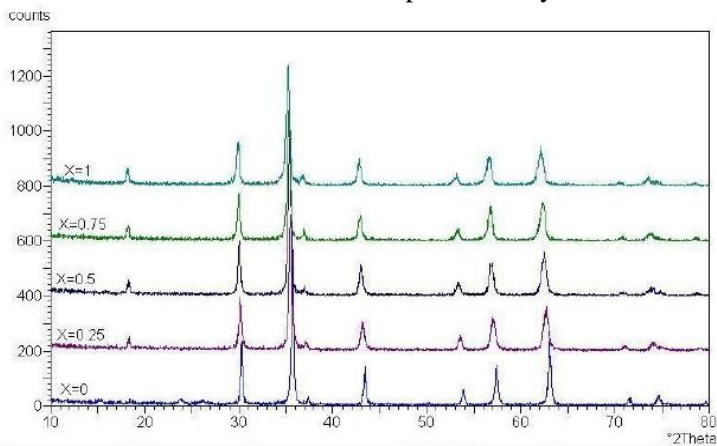


**Fig. (2):** X-ray diffraction patterns for the as prepared  $Li_{0.5-0.5x} Mn_x Fe_{2.5-0.5x} O_4$  nanopowders ;  $x=0, 0.25, 0.5, 0.75$  and  $1$ .

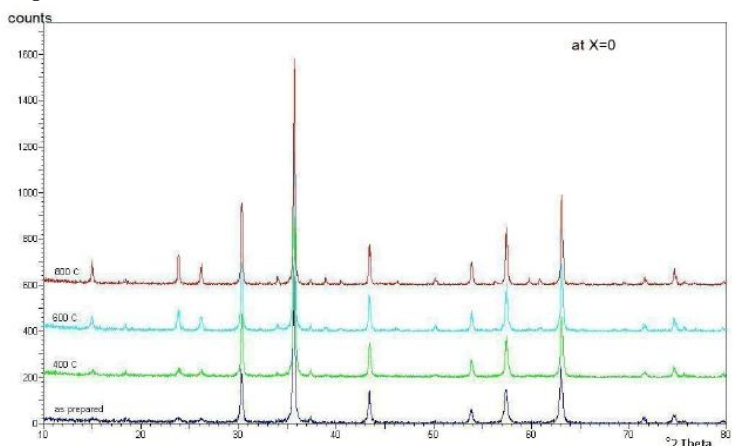


**Fig. (3):** X-ray diffraction patterns for  $Li_{0.5} Fe_{2.5} O_4$  nanopowders annealed at different temperatures ( $T_a=400, 600, 800\text{oC}$ ).

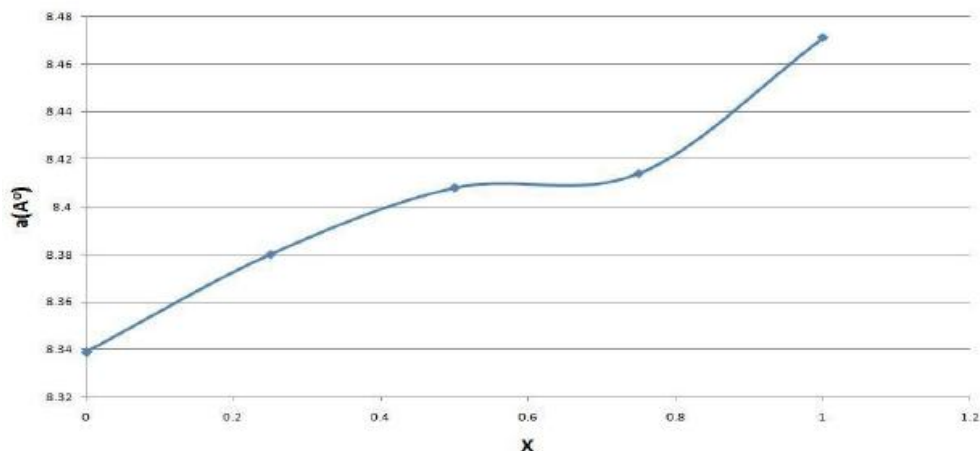


Fig. (4): Lattice parameter for the as prepared  $\text{Li}_{0.5-0.5x}\text{Mn}_x\text{Fe}_{2.5-0.5x}\text{O}_4$  nanopowders ;  $x=0, 0.25, 0.5, 0.75$  and  $1$ .

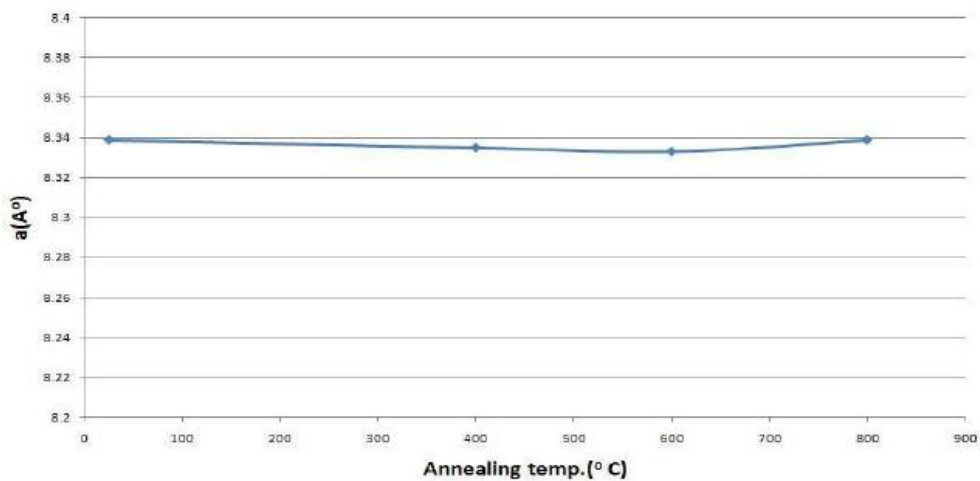


Fig. (5): Lattice parameter for  $\text{Li}_{0.5}\text{Fe}_{2.5}\text{O}_4$  nanopowders annealed at different temperatures ( $T_a=400, 600, 800^\circ\text{C}$ )

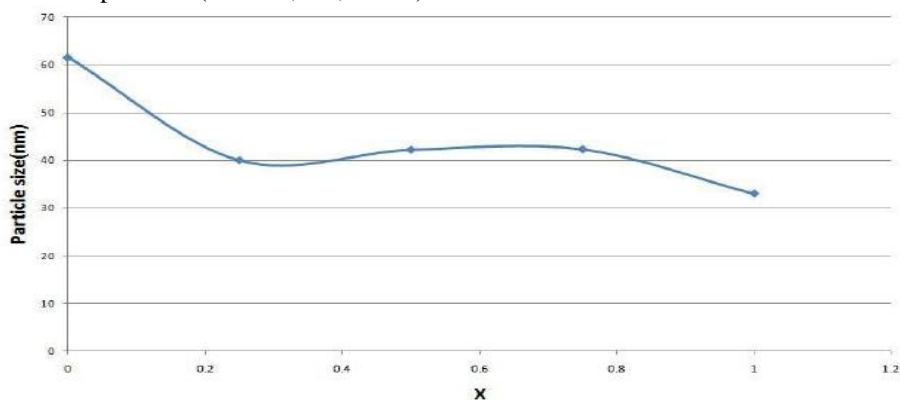
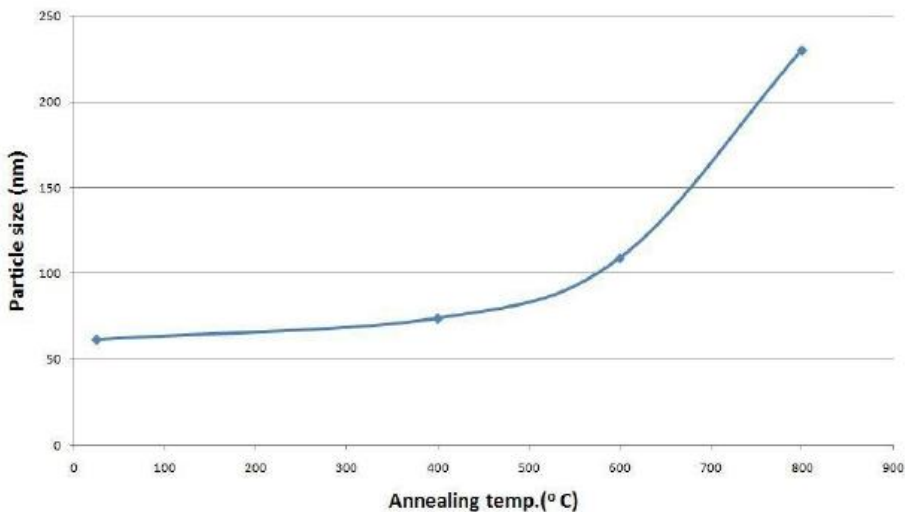


Fig. (6): Variation of Particle size for the as prepared  $\text{Li}_{0.5-0.5x}\text{Mn}_x\text{Fe}_{2.5-0.5x}\text{O}_4$  nanopowders ;  $x=0, 0.25, 0.5, 0.75$  and  $1$

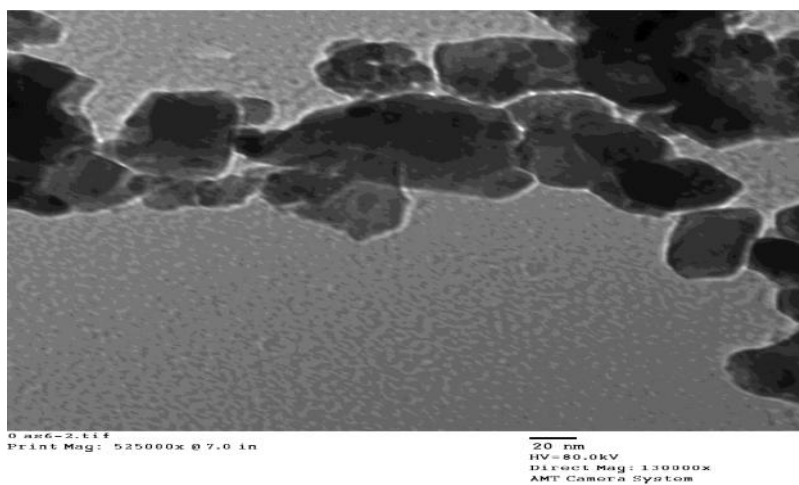
Figure (7), shows the variation of particle size, calculated from X-ray, with annealing temperature for  $\text{Li}_{0.5}\text{Fe}_{2.5}\text{O}_4$ . The particle size is found to increase with annealing temperature, which is due to the increase of coalescence with increasing annealing temperature. Fig.(8) (a), (c) and (b) shows the TEM images for the as prepared  $\text{Li}_{0.5}\text{Fe}_{2.5}\text{O}_4$  and  $\text{MnFe}_2\text{O}_4$  as well as  $\text{Li}_{0.5}\text{Fe}_{2.5}\text{O}_4$  annealed at  $800^\circ\text{C}$  respectively. The particles are found to be stacked on each other due to their mutual magnetic interactions. For  $\text{Li}_{0.5}\text{Fe}_{2.5}\text{O}_4$  annealed at  $T_a=800^\circ\text{C}$ , a well crystallinity is observed which is compatible with the X-ray results. The as prepared  $\text{Li}_{0.5}\text{Fe}_{2.5}\text{O}_4$  and  $\text{MnFe}_2\text{O}_4$  have average particle size calculated from TEM equal to 50 nm and 30 nm respectively which is roughly agrees with the XRD particle size. Different parameter of as prepared  $\text{Li}_{0.5-0.5x}\text{Mn}_x\text{Fe}_{2.5-0.5x}\text{O}_4$  system and their porosities are given in Table (1). The same parameters of  $\text{Li}_{0.5}\text{Fe}_{2.5}\text{O}_4$  annealed at different temperatures are shown in Table (2). From Table (1), it is clear that the total porosity decreased initially and then remained fairly constant for  $x=0.25, 0.5$  and  $0.75$  and then increased at  $x=1$ . The porosity results for as prepared  $\text{Li}_{0.5-0.5x}\text{Mn}_x\text{Fe}_{2.5-0.5x}\text{O}_4$  can be discussed in the light of the competition of the two types of porosities, inter porosity that depends on the particle size and intra porosity that depends on the ionic radius [27], where

$$P_{\text{tot.}}=P_{\text{inter}} + P_{\text{intra}} \quad (5)$$

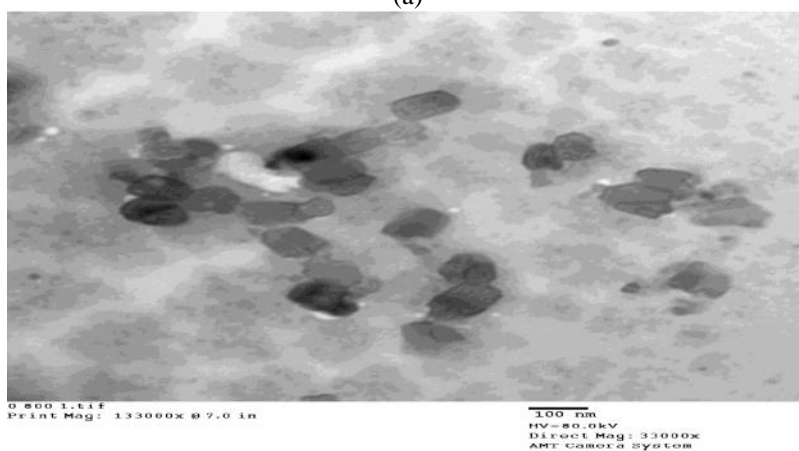
The initial decrease of the porosity of the as prepared  $\text{Li}_{0.5-0.5x}\text{Mn}_x\text{Fe}_{2.5-0.5x}\text{O}_4$  is due to the effect of  $P_{\text{inter}}$ , as the particle size decreased, while the constancy of  $P_{\text{tot.}}$  for  $x=0.25, 0.5$  and  $0.75$  is due to the competition between  $P_{\text{inter}}$  and  $P_{\text{intra}}$  and finally the increase of  $P_{\text{tot.}}$  at  $x=1$  can be attributed to the effect of  $P_{\text{intra}}$  due to the appreciable increase in the lattice parameter and the small decrease in the particle size (nearly about 9 nm). Generally, the porosity of annealed toroidal  $\text{Li}_{0.5}\text{Fe}_{2.5}\text{O}_4$  sample decreases, due to coalescence of particles and shrinkage of the samples.



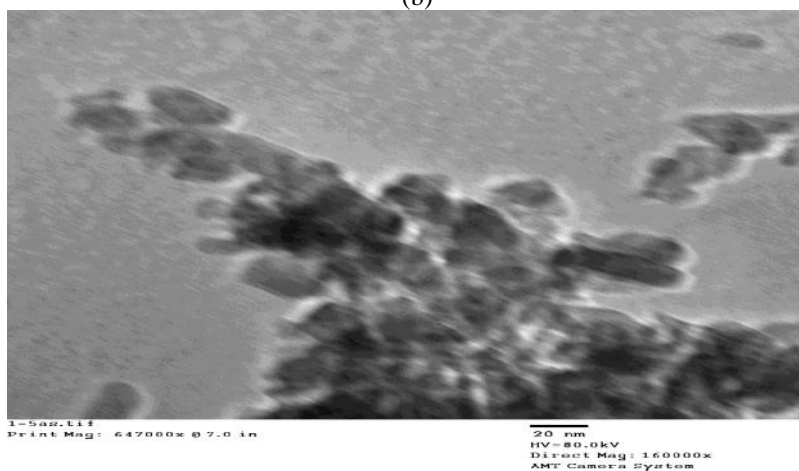
**Fig. (7):** Particle size for  $\text{Li}_{0.5}\text{Fe}_{2.5}\text{O}_4$  nanopowders annealed at different temperatures ( $T_a=400, 600, 800^\circ\text{C}$ ).



(a)



(b)



(c)

**Fig. (8):** TEM images for (a) as prepared  $\text{Li}_{0.5}\text{Fe}_{2.5}\text{O}_4$ , (b)  $\text{Li}_{0.5}\text{Fe}_{2.5}\text{O}_4$  annealed at  $T_a=800^\circ\text{C}$  and (c) as prepared  $\text{MnFe}_2\text{O}_4$ .

**Table (1):** Some Physical parameters for as prepared  $\text{Li}_{0.5-0.5x}\text{Mn}_x\text{Fe}_{2.5-0.5x}\text{O}_4$  nanopowder;  $x=0, 0.25, 0.5, 0.75$  and 1.

| Composition(x) | Lattice parameter, $A^\circ$ | Avg. particle size (nm) | X-ray density(dx), ( $\text{g}/\text{cm}^3$ ) | Porosity (P) (%) | Surface area (S), ( $\text{m}^2/\text{g}$ ) |
|----------------|------------------------------|-------------------------|---|------------------|---|
| 0              | 8.339                        | 61.6                    | 4.74  | 18.02            | 20.53                                       |
| 0.25           | 8.38                         | 40                      | 4.81  | 14.74            | 31.16                                       |
| 0.5            | 8.408                        | 42.2                    | 4.89  | 14.22            | 29.07                                       |
| 0.75           | 8.414                        | 42.3                    | 5.01  | 14.62            | 28.30                                       |
| 1              | 8.471                        | 33                      | 5.04  | 17.07            | 36.08                                       |

**Table (2):** Some physical parameters for  $\text{Li}_{0.5}\text{Fe}_{2.5}\text{O}_4$  nanopowder with different annealing temperatures ( $T_a=400,600,800^\circ\text{C}$ )

| Annealing temperature ( $T_a$ ) | Lattice parameter, $A^\circ$ | Avg. particle size (nm) | X-ray density(dx), ( $\text{g}/\text{cm}^3$ ) | Porosity (P) (%) | Surface area (S), ( $\text{m}^2/\text{g}$ ) |
|---------------------------------|------------------------------|-------------------------|---|------------------|---|
| 400 $^\circ\text{C}$            | 8.335                        | 74                      | 4.75  | 18.72            | 17.07                                       |
| 600 $^\circ\text{C}$            | 8.333                        | 109                     | 4.75  | 8.49             | 11.58                                       |
| 800 $^\circ\text{C}$            | 8.339                        | 230                     | 4.74  | 11.94            | 5.50  |

### 3.1.2. Infrared spectroscopy analysis.

Far infrared spectroscopy is an excellent tool to study the distribution of the cations in tetrahedral and octahedral sites in ferrite system [28]. The IR transmission bands for the as prepared  $\text{Li}_{0.5-0.5x}\text{Mn}_x\text{Fe}_{2.5-0.5x}\text{O}_4$  series are shown in Fig.(9). The bands in the region of (300-700  $\text{cm}^{-1}$ ) are assigned to the fundamental vibrations of the ferrites crystal lattice. From Fig.(9), it is clear that for  $x=0$ ,  $\nu_2$  and  $\nu_3$  bands are well separated. However by addition of  $\text{Mn}_{+2}$  -ion, overlapping occurs between  $\nu_2$  and  $\nu_3$  with minima in the range of (378-373  $\text{cm}^{-1}$ ). Furthermore, the minima shift to a lower wave number by increasing of  $\text{Mn}_{+2}$  -ion content. These results could be accounted for as follows: It is known that  $\nu_2$  band in most ferrites, appears in the range  $\approx(390-490\text{cm}^{-1})$  and is attributed to the vibrations of the high valency cation(s) occupying octahedral ( $\text{O}_h$ )-site such as ( $\text{Mn}_{+3}\text{-O}$  and  $\text{Fe}_{+3}\text{-O}$ ) bonds. Moreover  $\nu_3$  band appears in the range  $\approx(310-360\text{cm}^{-1})$  and is attributed to the vibrations of the low valency cation(s) occupying  $\text{O}_h$ -site such as ( $\text{Li}_{+1}\text{-O}$ ,  $\text{Mn}_{+2}\text{-O}$  and  $\text{Fe}_{+2}\text{-O}$ ) bonds [28-30]. Furthermore, metastable cation distribution occurs due to the nanosize particles [31]. So we find a lot of cations with different valencies occupying  $\text{O}_h$ -site [ $\text{Mn}_{+2}$ ,  $\text{Fe}_{+3}$ ,  $\text{Mn}_{+3}$ ,  $\text{Fe}_{+2}$  and  $\text{Li}_{+1}$ ], then the overlap occurs and the metastable cation distribution between A-site and B-site enhances such overlapping. The shift in minima of the overlapped peaks is attributed to the increase in lattice parameter which in turn increases the bond lengths and hence decreases the wave number. On the other hand, we found that the peak of  $\nu_1$  is splitted into two peaks with increasing  $\text{Mn}_{+2}$ -ion content, which coincide with the fact that the Mn-ions are distributed between A- and B-sites [32]. Furthermore, we noticed that  $\nu_4$  makes overlapping

by introducing Mn<sup>+2</sup>-ion which is the result of the competition between the overlapping occurs in O<sub>h</sub>-site and splitting occurs in tetrahedral (t<sub>h</sub>)-site, such that the overlapping effect overcomes. The data of IR are summarized in Table (3).

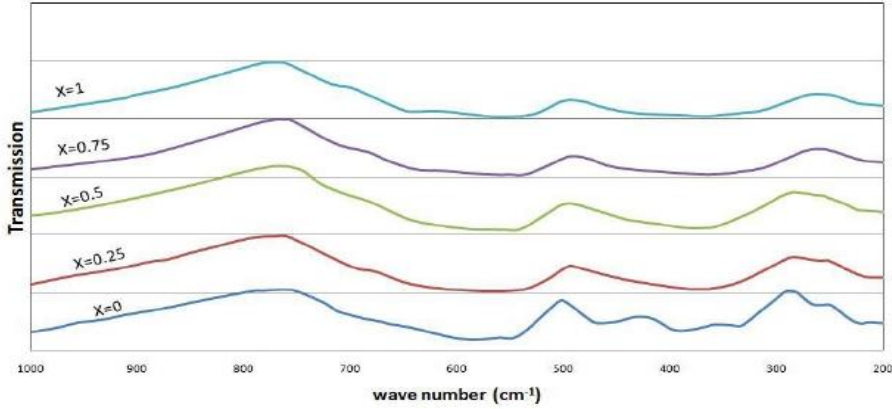


**Fig. (9):** Infrared transmission spectra for the as prepared Li<sub>0.5-0.5x</sub>Mn<sub>x</sub>Fe<sub>2.5-0.5x</sub>O<sub>4</sub> nanopowders ; x=0, 0.25, 0.5, 0.75 and 1 (T<sub>a</sub>=400,600,800oC)

**Table (3):** Effect of Mn<sup>+2</sup> on the IR transmission spectra of as prepared Li<sub>0.5-0.5x</sub>Mn<sub>x</sub>Fe<sub>2.5-0.5x</sub>O<sub>4</sub> nanopowder; x=0, 0.25, 0.5, 0.75 and 1.

| Composition(x) | v <sub>1</sub> (cm <sup>-1</sup> ) | v <sub>2</sub> (cm <sup>-1</sup> ) | v <sub>3</sub> (cm <sup>-1</sup> ) | v <sub>4</sub> (cm <sup>-1</sup> ) |
|----------------|------------------------------------|------------------------------------|------------------------------------|------------------------------------|
| 0              | 583                                | 464                                | 384-336                            | 266-226                            |
| 0.25           | 572                                | Overlapping with minima            |                                    | -                                  |
|                |                                    | 378                                |                                    |                                    |
| 0.5            | 561                                |                                    | 376                                | -                                  |
| 0.75           | 630-553                            |                                    | 369                                | -                                  |
| 1              | 635-554                            |                                    | 373                                | -                                  |

Figure (10) shows the IR transmission spectra of the annealed Li<sub>0.5</sub>Fe<sub>2.5</sub>O<sub>4</sub> sample at different temperatures 400,600 and 800<sup>o</sup>C. From Fig.(10) and Table (4), we can note that v<sub>1</sub>, v<sub>2</sub> and v<sub>3</sub> are nearly constant, which means that the annealing temperature does not affect the cation distribution of Li<sub>0.5</sub>Fe<sub>2.5</sub>O<sub>4</sub>, which agrees well with the lattice parameter results.

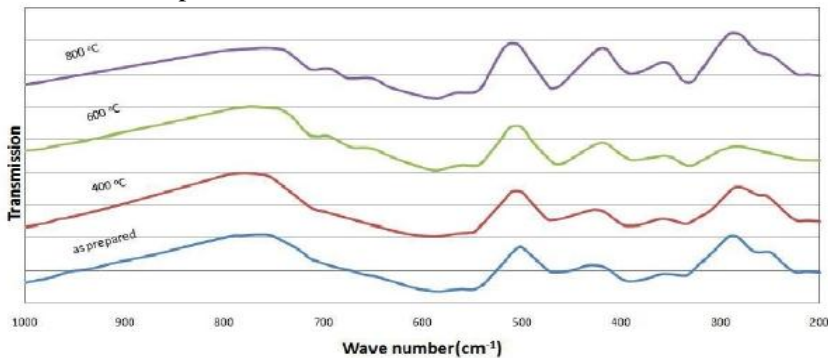


**Fig. (10):** Infrared transmission spectra for for Li<sub>0.5</sub>Fe<sub>2.5</sub>O<sub>4</sub> nanopowders annealed at different temperatures

**Table (4):** Effect of annealing temperature on the IR transimition spectra of  $\text{Li}_{0.5}\text{Fe}_{2.5}\text{O}_4$  nanopowder at ( $T_a=400,600,800^\circ\text{C}$ ).

| Annealing temperature ( $T_a$ ) | $\nu_1(\text{cm}^{-1})$ | $\nu_2(\text{cm}^{-1})$ | $\nu_3(\text{cm}^{-1})$ | $\nu_4(\text{cm}^{-1})$ |
|---------------------------------|-------------------------|-------------------------|-------------------------|-------------------------|
| 400°C                           | 585                     | 465                     | 378-336                 | 262-225                 |
| 600°C                           | 585-551                 | 465                     | 387-331                 | 220                     |
| 800°C                           | 587-552                 | 468                     | 389-334                 | 262-223                 |

### 3.2. Magnetization results analysis.

The hysteresis curves (M-H) for the as prepared  $\text{Li}_{0.5-0.5x}\text{Mn}_x\text{Fe}_{2.5-0.5x}\text{O}_4$  samples and  $\text{Li}_{0.5}\text{Fe}_{2.5}\text{O}_4$  nanopowder ferrites annealed at different temperature are shown in Fig. (11 and 12) respectively. For the as prepared Li-Mn ferrite samples, the hysteresis parameters such as saturation magnetization ( $M_s$ ), coercivity ( $H_c$ ) and retentivity ( $M_r$ ) determined from the hysteresis graphs, are given in Table.5. It is clear that the saturation magnetization initially increases till  $x=0.5$  then by further increase of  $\text{Mn}_{+2}$ -ion concentration, the saturation magnetization decreases. This behavior could be explained as follows: According to Neel theory, the magnetization is given by ( $M_s=2.5+2.5x$ ), where it is assumed the cation distribution to be ( $\text{Mn}_{0.8x}\text{Fe}_{1-0.8x}$ ) [ $\text{Li}_{0.5-0.5x}\text{Mn}_{0.2x}\text{Fe}_{1.5+0.3x}$ ] $\text{O}_4$  and 80% of  $\text{Mn}_{+2}$ -ions occupy the tetrahedral sites, as in the case of bulk ferrites[32]. According to the M(x) relation, the magnetization should increase with (x) which agrees with the experimental results up to  $x=0.5$ .

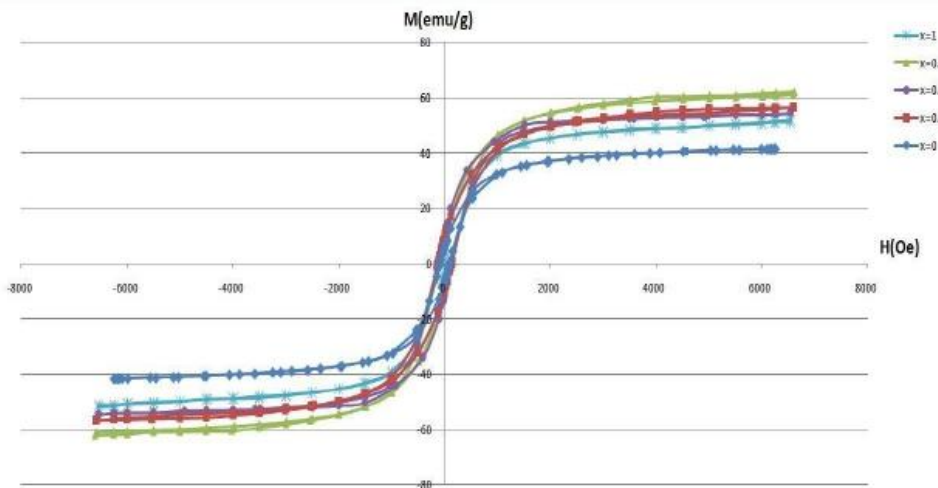


**Fig. (11):** Hysteresis curves for the as prepared  $\text{Li}_{0.5-0.5x}\text{Mn}_x\text{Fe}_{2.5-0.5x}\text{O}_4$  nanopowders;  $x=0. 0.25, 0.5, 0.75$  and  $1$

**Table (5):** Hysteresis magnetization parameters and Curie temperature of  $\text{Li}_{0.5-0.5x}\text{Mn}_x\text{Fe}_{2.5-0.5x}\text{O}_4$  as prepared nanopowder with ( $x=0.0.25, 0.5, 0.75, 1$ ).

| Composition(x) | $M_s(\text{emu/g})$ | $H_c(\text{Oe})$ | $M_r(\text{emu/g})$ | $T_c(^\circ\text{C})$ |
|----------------|---------------------|------------------|---------------------|-----------------------|
| 0              | 41.61               | 87.65            | 6.29                | 632.6                 |
| 0.25           | 56.70               | 122.02           | 9.45                | 585.7                 |
| 0.5            | 61.11               | 104.83           | 8.10                | 525.1                 |
| 0.75           | 57.75               | 104.34           | 8.01                | 473.7                 |
| 1              | 51.20               | 84.21            | 4.14                | 486.95                |

The decrease of  $M_s$  with increase of Mn concentration ( $x$ ) may be attributed to the appearance of Yafet-Kittel angle in B-sites. It is known that the condition for the presence of Yafet-Kittel angle in B-site is that the B-B interaction must be comparable with A-B interactions. This condition seems to fulfill in our system for higher Mn concentration which corresponds to increase of both Mn and Fe ions in B-site (ions of  $5 \mu_B$ ) and meanwhile a decrease of Li concentration. This allows the magnetic interactions in B-site to increase i.e. B-B interaction increases and Yafet-Kittel angle appears and accounts on the decrease of magnetization for high Mn concentration [32 and 33]. In fact the occurrence of the Yafet-Kittel angle in B-site will be most probable if either Mn or Fe ions migrate from A- to B-sites.

The coercivity  $H_c$  in multidomain structure depends on many factors such as the porosity, the anisotropy constant  $K_1$  and particle size  $L$ . It was reported that  $H_c$  is directly proportional to both the porosity and the anisotropy constant and is inversely proportional to the particle size through the relation  $H_c = g \cdot h / L^{3/2}$ ; where  $g$  and  $h$  are constants and  $L$  is the particle size [34].

For as prepared  $\text{Li}_{0.5-0.5x}\text{Mn}_x\text{Fe}_{2.5-0.5x}\text{O}_4$ , it is obvious from Table (5) that  $H_c$  initially increased, then it decreased and remained constant till  $x=0.75$  and finally it decreased again. This behavior can be interpreted in the light of the previous parameters where  $K_1$  which results from  $\text{Fe}^{2+}$  ions decreases with  $x$ . Thus for  $x = 0.25$ , the particle size seems to be the dominant factor as the particle size decreased from 60 nm to 42 nm as shown in Table (1). The decrease in  $H_c$  can be attributed to the anisotropy effect where both the porosity and particle size are nearly constant.

The constancy of  $H_c$  at  $x=0.5$  and  $0.75$  results from the competition between the porosity, the particle size and anisotropy effect. Finally, at  $x=1$  the decreasing in  $H_c$  may be attributed mainly to the effect of  $K_1$  as both the particle size and porosity tend to increase  $H_c$ .

For the annealed samples of  $\text{Li}_{0.5}\text{Fe}_{2.5}\text{O}_4$  at different temperatures 400, 600, 800°C, it can be clearly noticed that the increase in annealing temperature from 400 to 800°C causes an increase in the loop area leading to a changing in its parameters. The increase in saturation magnetization for the annealed samples of  $\text{Li}_{0.5}\text{Fe}_{2.5}\text{O}_4$  is obvious from Fig.12 and Table (6), that is may be due to the phase purity and well defined crystallinity [26]. As for  $H_c$ , it is initially increased and then it decreased by increasing the annealing temperature. The increase of  $H_c$  can be attributed to the fact that at a critical particle size of the single domain structure,  $H_c$  attains a maximum value. So we can apparently assume that the critical particle size for lithium ferrite at ( $T_a=400^\circ\text{C}$ ) is ( $\approx 74$  nm). The increase of porosity at this region confirms this result. The decrease of  $H_c$  at ( $T_a=600^\circ\text{C}$  and  $800^\circ\text{C}$ ) is due to the increase in particle size (exceeding the critical particle size for single domain structure), i.e. the particle sizes are in multidomain structure region, at which  $H_c$  is inversely proportional with particle size as aforementioned.

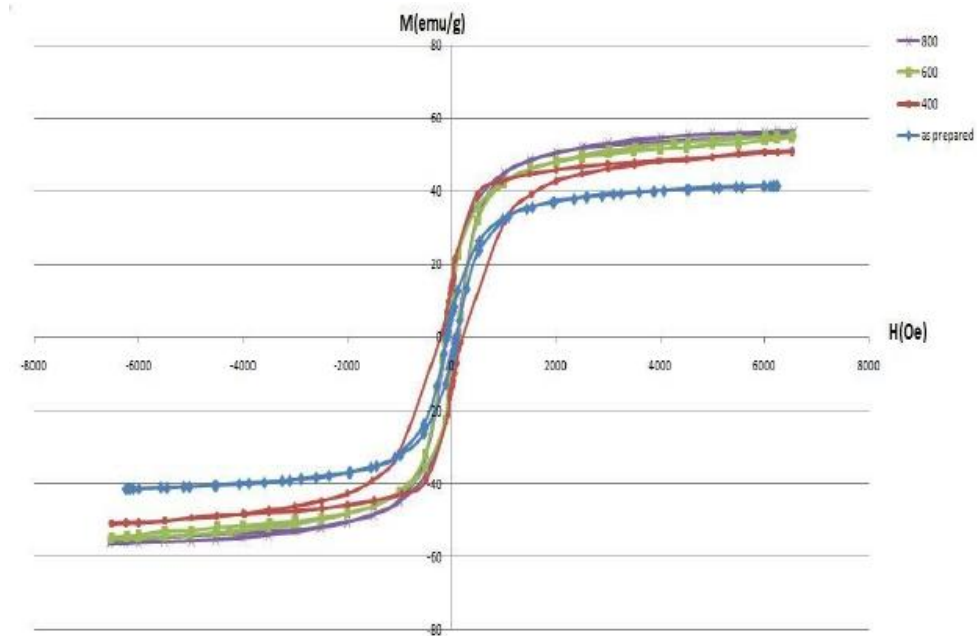


**Fig. (12):** Hysteresis curves for  $\text{Li}_{0.5}\text{Fe}_{2.5}\text{O}_4$  nanopowders annealed at different temperatures ( $T_a=400, 600, 800^\circ\text{C}$ )

**Table (6):** Hysteresis magnetization parameters and Curie temperature of  $\text{Li}_{0.5}\text{Fe}_{2.5}\text{O}_4$  nanopowder at ( $T_a=400, 600, 800^\circ\text{C}$ ).

| Annealing temperature ( $T_a$ ) | $M_s$ (emu/g) | $H_c$ (Oe) | $M_r$ (emu/g) | $T_c$ ( $^\circ\text{C}$ ) |
|---------------------------------|---------------|------------|---------------|----------------------------|
| 400 $^\circ\text{C}$            | 49.64         | 214.04     | 14.21         | 636.3                      |
| 600 $^\circ\text{C}$            | 54.86         | 125.46     | 9.11          | 638.5                      |
| 800 $^\circ\text{C}$            | 56.02         | 118.58     | 9.06          | 625.3                      |

The Curie temperatures of the as prepared  $\text{Li}_{0.5-0.5x}\text{Mn}_x\text{Fe}_{2.5-0.5x}\text{O}_4$  samples and annealed  $\text{Li}_{0.5}\text{Fe}_{2.5}\text{O}_4$  nanopowder ferrite samples are determined from the initial permeability measurements and are tabulated in Tables (5 and 6) respectively. It is known that Curie temperature is affected by many factors such as the relative concentrations of the moments on both sites ( $N_A/N_B$ ) and the distance between A- and B-sites which in turn is affected by the variation of the lattice parameter, i.e. as lattice parameter increases then  $T_c$  will decrease [35]. Accordingly, for  $\text{Li}_{0.5-0.5x}\text{Mn}_x\text{Fe}_{2.5-0.5x}\text{O}_4$  system, the decrease of Curie temperature  $T_c$  with increasing  $\text{Mn}_{+2}$ -ion concentration, as shown in Fig.(13), can be attributed to the effect of lattice parameter which is increased by increasing  $\text{Mn}_{+2}$ -ion concentration. For the annealed  $\text{Li}_{0.5}\text{Fe}_{2.5}\text{O}_4$  samples, the Curie temperature  $T_c$  is more or less constant which is the expected behavior as the lattice constant and relative concentrations of ions on A- and B- sites are invariant.

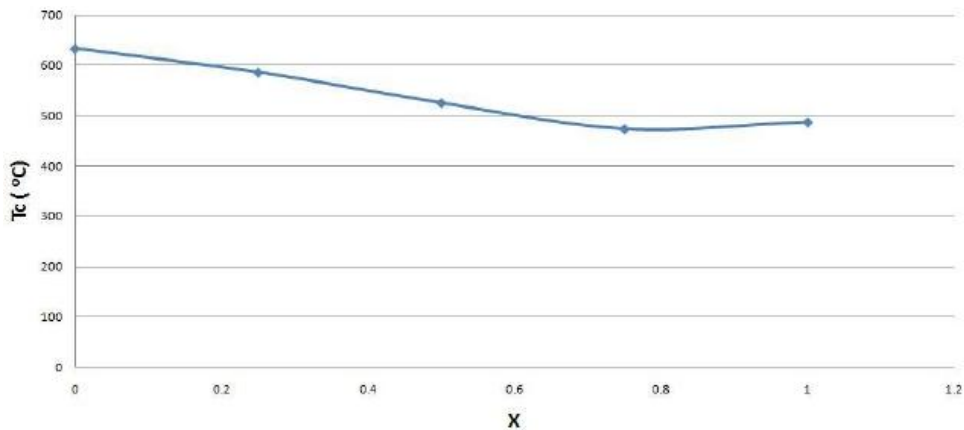


**Fig. (13):** Curie temperature for the as prepared  $\text{Li}_{0.5-0.5x}\text{Mn}_x\text{Fe}_{2.5-0.5x}\text{O}_4$  nanopowders ;  $x=0, 0.25, 0.5, 0.75$  and  $1$

#### 4. Conclusion

The effect of  $\text{Mn}_{+2}$ -ion substitution on the physical and magnetic properties of the as prepared  $\text{Li}_{0.5-x}\text{Mn}_x\text{Fe}_{2.5-x}\text{O}_4$  nanopowder;  $x=0, 0.25, 0.5, 0.75$  and  $1$  and  $\text{Li}_{0.5}\text{Fe}_{2.5}\text{O}_4$  nanopowder annealed at different temperatures ( $T_a=400, 600, 800^\circ\text{C}$ ), prepared by the sol-gel autocombustion method, have been investigated. It was found that the addition of  $\text{Mn}_{+2}$ -ion to the Li-ferrite increases the lattice parameter due to the difference in ionic radii while the particle size decreased. The saturation magnetization increased at first till  $x=0.5$  then by further increase of  $\text{Mn}_{+2}$ -ion the saturation magnetization decreased. Also it has been observed that Curie temperature generally decreased vigorously by addition of  $\text{Mn}_{+2}$ -ion. The effect of annealing temperature on the physical and magnetic properties for  $\text{Li}_{0.5}\text{Fe}_{2.5}\text{O}_4$  do not show a significant impact. The experimental results obtained are of interest for the research and development of compositionally modified soft magnetic ferrite for various industrial applications.

#### References:

1. E. Wolska, K. Stempin, O. Krasnowska-Hobbs. *Solid State Ionics*, **101**, 527 (1997).
2. M.N. Obrovac, O. Mao, J.R. Dahn. *Solid State Ionics*, **112**, 9 (1998).
3. Y. Sakurai, H. Arai, J. Yamaki. *Solid State Ionics*, **113**, 29 (1998).
4. J.R. Dahn, U. Vomsacken, C.A. Micha. *Solid State Ionics*, **44**, 87 (1990).
5. Y.S. Cho, Y.L. Burdick, V.R.W. Amarakoon. *J. Am. Ceram. Soc.*, **82**, 1416 (1999).
6. P.S. Anil Kumar, J.J. Shrotri, S.D. Kulkarni, C.E. Deshpande, S.K. Date. *Mater.Lett.*, **27**, 293 (1996).
7. P.D. Baba, G.M. Argentina, *Microw. Theory Technol.* **22**, 654 (1974).
8. I.Z. Rahman, T.T. Ahmed. *J. Magn. Magn. Mater.*, **290**, 1576 (2005).

9. P. Sainamthip, V.R. W. Amarakoon. *J. Am. Ceram. Soc.*, **71(2)**, C92 (1988).
10. S. Komarneni, E. Fregeau, E. Breval, R.Roy. *J. Am. Ceram. Soc.*, **71(1)**, C26 (1988).
11. A.R. Bueno, M.L. Gregori, M.C.S.N0obrega., *Mater. Chem. Phys.*, **105**, 229 (2007).
12. A.Verma, R. Chatterjee. *J. Magn. Magn. Mater.*, **306**, 313 (2006).
13. Yen-Pei Fu, Chin-Shang Hsu, *Solid State Commun.*, **134**, 201 (2005).
14. Xiwei Qi , Ji Zhou, Zhenxing Yue, Zhilun Gui, Longtu Li. *Mater. Sci. Eng.*, **B99**, 278 (2003).
15. Yen-Pei Fu, Shen Tsao, Chen-Ti Hu, Yeong-Der Yao, *J. Alloys Compds*, **395**, 272 (2005).
16. P.P. Hankare, R.P. Patil, U.B. Sankpal, S.D. Jadhav, I.S. Mulla, K.M.Jadhav, B.K. Chougule . *J. Magn. Magn. Mater.*, **321**, 3270 (2009).
17. H. Waqas , A. H. Qureshi, *J. Therm. Anal. Calorim.*, **100**, 529 (2010).
18. H. Waqas , A. H. Qureshi. *J. Therm. Anal. Calorim.*, **98**, 355 (2009).
19. Souzana Lorentzou, Christos C. Agrafiotis, Athanasios G. Konstandopoulos. *Granul. Matter.*, **10**, 113 (2008).
20. B.D.Cullity, Elements of X-ray Diffraction, second printing, Addison Wesley Publishing Company, Inc, USA, (1959).
21. B.D. Cullity, Elements of X-ray Diffraction, Addison-Wesley, Reading, MA, (1978).
22. Xiwei Qi, Ji Zhou, Zhenxing Yue, Zhilun Gui, Longtu Li. *Mater. Sci. Eng.*, **B99**, 278 (2003).
23. R. D. Shannon. *Acta Crystallographica.*, **A32**, 751 (1976).
24. M.K. Shobana, S.Sankar. *J. Magn. Magn. Mater.*, **321**, 2125 (2009).
25. M.K. Shobana, S. Sankar. *J. Magn. Magn. Mater.*, **321**, 599 (2009).
26. G. Gnanaprakash, John Philip, *Baldev Raj. Mater. lett.*, **61**, 4545 (2007).
27. Kigery W.D., Bowen H.K., Uhlmann D.R., Introduction of ceramics, John Wiley and Sons , NewYork , London (1996).
28. R.D. Waldron. *Phys., Rev.*, **99**, 1727 (1955).
29. P. Tarte and J. Preudhomme. *Spectrochim. Acta*, **A27**, 961 (1971).
30. B. Ramesh, D. Ravinder. *Mater., Lett.*, **62**, 2043 (2008).
31. RAJESH IYER, RUCHA DESAI and R V UPADHYAY. *Bull., Mater., Sci.*, **32**, 141 (2009).
32. C. Wende, Kh. Olimov, H. Modrow, F.E. Wagner, H. Langbein. *MATER. RES. BULL.* **41**, 1530 (2006).
33. P.P. Hankare,R.P. Patil, U.B. Sankpal, S.D. Jadhav, P.D. Lokhande, K.M. Jadhav. *J. Solid State Chem.*, **182**, 3217 (2009).
34. C. Kittel, *Phys. Rev.*, **70**, 965 (1946).
35. B.D. Cullity, Introduction to Magnetic Materials, Addison-Wesley, New York, (1972) p. 386.
36. Chickazumi S., Charap S., Physics of magnetism, John Wiley & Sons, New York. London. Sydney (1964).